

The onset of photometric variability in red giant stars^{*}

A. Jorissen^{1,**,} N. Mowlavi^{2,} C. Sterken^{3,***,} and J. Manfroid^{4,†}

¹ Institut d’Astronomie et d’Astrophysique, Université Libre de Bruxelles, CP 226, Boulevard du Triomphe, B-1050 Bruxelles, Belgium

² Observatoire de Genève, CH-1290 Sauverny, Switzerland

³ Vrije Universiteit Brussel, Pleinlaan 2, B-1050 Brussel, Belgium

⁴ Institut d’Astrophysique, Université de Liège, Av. de Coïnte 5, B-4000 Liège, Belgium

Received 16 July 1996 / Accepted 10 February 1997

Abstract. The onset of variability in red giant stars is studied from the data collected by the ‘Long-Term Photometry of Variables’ project which operates at ESO (La Silla) since 1982. The differential nature of the observations combined with a multi-night reduction algorithm enables to study the variability of over 50 red giants with an accuracy of the order of 2 to 3 millimag on time scales ranging from days to years. All red giants with spectral types late G to early K (i.e. $b - y \sim 0.6 - 0.8$) are stable at the level $\sigma_y < 6$ millimag (where σ_y is the standard deviation of the Strömgen y magnitude). Red giants with later spectral types are all variable, and it is found that the minimum variability level $\sigma_{y,\min}$ increases with increasing $b - y$, thus defining a *minimum-variability boundary*. The new data obtained in this paper reveal that the time scale of the associated variability increases with increasing $b - y$ (and thus amplitude), and that the stability of this time scale improves concomitantly. More precisely, irregular variations on time scales of 5 to 10 days (and $\sigma_y \sim 7$ millimag) characterize red giants with $b - y \sim 1.0$, whereas the variations (with $\sigma_y \sim 100$ millimag) become more regular with periods of the order of 50 d for red giants with $b - y \sim 1.3$. A radial-velocity jitter (of the order of 1.5 km s⁻¹ r.m.s.) is associated with this photometric variability, and suggests that stellar oscillations may be responsible for the observed variations.

Key words: stars: late-type – stars: variable: other – stars: oscillations

1. Introduction

Photometric variability is a common feature among red giant stars. The Mira variables are certainly the most spectacular

among these (‘mira’ stands for the latin word ‘wonderful’), with their visual amplitude reaching several magnitudes and with periods of several hundred days. Smaller amplitudes and shorter periods are found among the semi-regular (SR) and irregular (L) variables, so that a continuous range in visual amplitudes actually exists. An important -and yet unresolved- question for the study of stellar structure is to understand how the photometric variability grows as the star evolves along the giant branch. Or, in other words, is it possible to trace the evolution of a red giant star by the tendencies observed in its photometric properties? Important clues in this respect have been provided by Grenon (1993), Eyer et al. (1994), and more recently by Edmonds & Gilliland (1996). The analysis of the whole sample of stars measured in the Geneva photometric system (Grenon 1993) and of the preliminary photometric data provided by the Hipparcos satellite after the first 1.5 y of the mission (Eyer et al. 1994) leads to the conclusion that late GIII stars are stable at the level 3 10^{-3} mag (3 millimag) in the V or H_p bands, whereas K and M giants are increasingly variable as their luminosity increases or effective temperature decreases. No information on the lightcurve is given, however. From a photometric analysis of K giants in the globular cluster 47 Tuc, using the *Hubble Space Telescope*, Edmonds & Gilliland (1996) have refined this picture by showing that these giants are variable on time scales of a few days with semi-amplitudes of 10 – 30 millimag in the U band. Because their observations lasted for only 38 hours (1.6 d), variable stars with longer periods could not be detected. This selection effect causes the detected K giant variables to be restricted to an *apparent* ‘instability strip’, since variable stars of later spectral types do actually exist but vary on longer time scales, as shown in this paper.

In the present paper, the onset of variability in red giant stars is studied with unprecedented accuracy, and the first lightcurves of microvariable K and M giants are presented. The relationship between the amplitude and the time scale of the variations is also investigated for the first time. Use is made of the database of the ‘Long-Term Photometry of Variables’ (LTPV) project, that operates since 1982 at the European Southern Observatory (La Silla, Chile). These data are especially well suited to this pur-

Send offprint requests to: A. Jorissen

^{*} Based on observations carried out at the European Southern Observatory (ESO, La Silla, Chile), and at the Swiss telescope at the Haute Provence Observatory (France)

^{**} Research Associate, FNRS, Belgium

^{***} Senior Research Associate, NFWO, Belgium

[†] Research Director, FNRS, Belgium

pose, since (i) the differential nature of the observations coupled with a multi-night reduction algorithm yields an accuracy of 2 to 3 millimag in the Strömgren y band over a decade, (ii) the time sampling of the observations allows to investigate variations on time scales from days to years, and (iii) over 50 different red giant stars have been monitored by the LTPV project. A detailed description of the LTPV project is given in Sect. 2. Section 3 investigates the $(\sigma_y, b - y)$ diagram, while Sect. 4 reveals the existence in that diagram of a lower σ_y boundary increasing with $b - y$ (the *minimum-variability boundary*). Section 5 investigates the relationship between the amplitude and the time scale of the variations. Section 6 discusses the concomitant radial velocity variations, while Sect. 7 briefly suggests possible physical mechanisms for the observed variations. Conclusions are presented in Sect. 8.

2. The LTPV data set

The LTPV project is a collaborative effort involving several groups of astronomers interested in the long-term monitoring of various classes of variable stars (Sterken 1983, 1994). It operates since 1982 at the European Southern Observatory (ESO) on the ESO 50 cm, Bochum 61 cm and Danish 50 cm telescopes (from December 1987 on, the latter being referred to as Strömgren Automatic Telescope, SAT), in the Strömgren *woby* system. Observing runs were typically one month-long (each period involving a different observer), with an average of 6 runs per year. About 230 different stars, grouped into 9 different sections (1: Pre-main sequence stars, 2: Ap stars, 3: Eclipsing binaries, 4: Be stars, 5: Supergiants, 6: X-ray sources, 7: Targets of opportunity, 8: Peculiar late-type stars, 9: Wolf-Rayet stars), were observed with a frequency ranging from 1 observation per night to 1 per month, depending on the variability type. The complete database containing about $120 \cdot 10^3$ measurements is available at the *Centre de Données Stellaires* (Strasbourg, France) and is documented in Manfroid et al. (1991), Sterken et al. (1993), Manfroid et al. (1994) and Sterken et al. (1995).

The observations are basically differential, each observation consisting in a sequence like APB or $APBPBA$, where P designates the program star, and A and B nearby comparison stars. A thorough description of the multi-night reduction algorithm can be found in Sterken & Manfroid (1992). The algorithm uses every measurement of every constant star and of every standard star to derive the extinction coefficients. Data from different instrumental systems are treated separately. The coefficients of the color matrix are computed at once using all the available data in a given instrumental system. This process, continuously updating the data sets, also prevents inter-run offsets that may otherwise occur for stars with extreme colors, like the red giants considered in this study. In fact, the results presented in this paper make use exclusively of data obtained with the SAT. These data are of higher accuracy than those obtained on the other two telescopes, mainly because the SAT is equipped with a *multichannel woby* photometer featuring four uncooled EMI9789QB tubes (Florentin Nielsen 1983). Moreover, the large body of data obtained in that system (denoted as 7

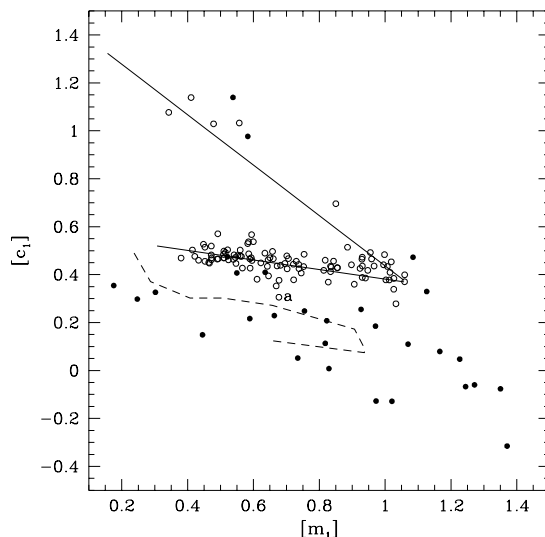


Fig. 1. The reddening-free $([m_1], [c_1])$ diagram for the sample of red giant stars extracted from the LTPV database as indicated in the text. Peculiar red giants (barium, S and carbon stars), whose photometric indices are altered by their chemical peculiarities, are represented by filled circles. Label *a* identifies the CN-strong giant HD 184944 (see text). The fiducial sequences for late-type main sequence stars and normal red-giant stars, as derived from Olsen (1984), are represented by the dashed and solid lines, respectively

or N in the LTPV catalogues) makes it possible to find adequate standards in the natural SAT system. No color transformation has thus been applied to the SAT data, which are expressed in the natural system (see Manfroid et al. 1994 for more details).

A complete statistical analysis of the LTPV database is in preparation. The current paper is restricted to the study of the intrinsic variability of red giant stars. Therefore, known eclipsing binaries, symbiotic and VV Cep stars, T Tau, RS CVn, R CrB and Cepheid variables have been removed from the LTPV subsample considered here. The spectral type of the remaining stars having $b - y \geq 0.5$ has then been checked in the SIMBAD database (priority being given to the revised Michigan spectral class, when available; Houk & Cowley 1975). Stars with spectral types earlier than G, or luminosity class V, or classified as G or K supergiants, have been removed from the final sample as well. Among the remaining G, K and M stars, about 25% have no luminosity class available, however. They have nevertheless been included in the final sample, since they fall along the red-giant fiducial sequence in the reddening-free $([m_1], [c_1])$ diagram discussed below.

The reddening-free $([m_1], [c_1])$ diagram indeed provides an efficient way of distinguishing late-type main sequence stars from non-chemically-peculiar red giants, as indicated by e.g. Olsen (1984; his Fig. 11). In the natural SAT system used throughout this paper, the reddening-free indices $[m_1]$ and $[c_1]$ are defined as

$$\begin{aligned} [m_1] &= m_1 + 0.21(b - y) \\ [c_1] &= c_1 + 0.35(b - y). \end{aligned} \quad (1)$$

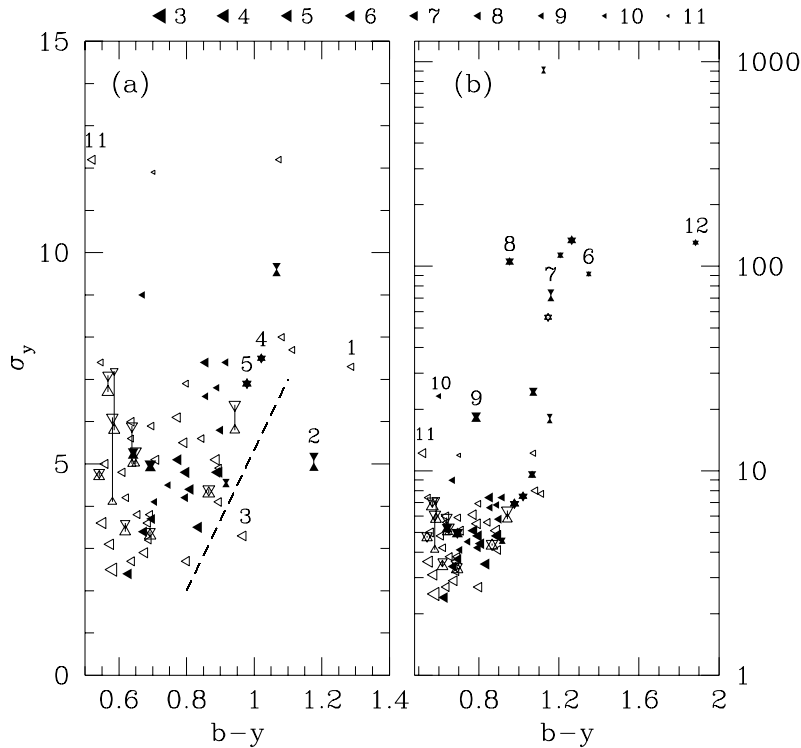


Fig. 2a and b. The $(\sigma_y, b - y)$ diagram for the sample of red giant stars extracted from the LTPV database as described in the text, σ_y (in 10^{-3} mag) being the standard deviation of the *differential* y magnitude. Filled symbols refer to peculiar red giant stars (barium, S or C stars). The size of the symbols reflects the magnitude of the faintest star in the pair, as illustrated on the top line. A vertical line connects the σ_y of the two pairs involving the variable star in the *APB* triplet, whereas the σ_y of the constant pair is drawn at the $b - y$ index of the reddest star in the pair (see text). Panel **a** is a zoom of panel **b**. The dashed line in panel **a** corresponds to the lowest standard deviation found at a given intrinsic (i.e. unreddened) $b - y$ index (the *minimum-variability boundary*). Stars 1, 2 and 3 in panel **a** are strongly reddened stars, and move to the left of the minimum-variability boundary after correcting for their color excess (see text). They have not been represented in panel **b**. Stars discussed in the text have been labelled as follows: 1: HD 161406; 2: HD 178717; 3: HR 7007; 4: HD 60197; 5: HD 44896; 6: BD-08° 1900; 7: BD-21° 5435; 8: HD 52432; 9: HD 182040; 10: HD 165929; 11: HD 100122; 12: BD-10° 1334

This definition directly results from the reddening path in the natural SAT system:

$$\begin{aligned} m_1 - m_0 &= -0.21 E_{b-y} \\ c_1 - c_0 &= -0.35 E_{b-y}, \end{aligned} \quad (2)$$

where $E_{b-y} = [(b - y) - (b - y)_0]$ is the color excess, and subscript 0 refers to unreddened indices. Equations (2) are obtained by transforming the reddening path provided by Crawford & Mandwewala (1976) from the standard *uvby* system to the natural SAT system, according to the transformation equations provided by Sterken et al. (1995; their Eq. 7). The latter equations were also used to transform the fiducial sequences provided by Olsen (1984; his Fig. 11) for late-type main-sequence stars and red-giant stars, and the resulting sequences in the natural SAT system are plotted in Fig. 1.

It appears that the red-giant fiducial sequence nicely fits the colors of the stars making up our final sample. Note that peculiar red-giant stars, like barium, S and carbon stars represented by filled circles in Fig. 1, should not be involved in this comparison, as their chemical peculiarities alter their colors. The same remark applies to the star labelled *a* (= HD 184944) in Fig. 1, since it is known to be a CN-strong giant star (Schmitt 1971). It may thus be concluded from Fig. 1 that our final sample exclusively contains red-giant stars, as opposed to main-sequence stars.

3. The $(\sigma_y, b - y)$ diagram

Since all the LTPV observations consist in sequences like *APA*, *APB*, *APBPBPA*..., we deal in this paper only with *differential* magnitudes (corresponding to the pairs $P - A$, $P - B$,

and $A - B$). The analysis is moreover restricted to the y band, which is, for red-giant stars, the most accurate one among the *uvby* bands.

For a given triplet consisting of a program star P and two comparison stars A and B , with N observing sequences *APB* ($y_A(k)$, $y_P(k)$, $y_B(k)$, $k = 1, N$) available over the time span of the monitoring, the standard deviation of the differential magnitude in the y band for the pair $s - t$ (where s and t stand for P , A or B) is defined as

$$\sigma_{y,s-t} = \frac{1}{N^{\frac{1}{2}}} \left(\sum_{k=1}^N [y_s(k) - y_t(k) - (\bar{y}_s - \bar{y}_t)]^2 \right)^{\frac{1}{2}}, \quad (3)$$

where \bar{y}_s stands for the average y magnitude of star s . In the case that P is much more variable than A and B (which is often, though not always, the case), we have $\sigma_{y,P-A} \sim \sigma_{y,P-B} \gg \sigma_{y,A-B}$.

The present study has been conducted on a sample of red giants with no external cause of variability (thus excluding known RS CVn, R CrB... variables as discussed in Sect. 2) and with more than 20 measurements spanning at least 1000 days. Figure 2 presents the $(\sigma_y, b - y)$ diagram for that sample. In that figure, the standard deviations of the two pairs involving the variable star in the *APB* triplet are connected with a vertical line, drawn at the $b - y$ value corresponding to the variable star, while the standard deviation of the pair involving the two least variable stars (A and B in most, though not all, cases) is represented by a single symbol drawn at the $b - y$ value of the reddest star in the pair.

Several interesting features are noticeable in Fig. 2:

(i) At $b - y < 0.8$ (corresponding to spectral types earlier than

about K3III; Ardeberg & Lindgren 1985), red giants are stable at the level $\sigma_y \leq 6$ millimag. The lower boundary observed around 3 millimag probably reflects the overall accuracy of our data, and is thus not significant. A small number of stars (HD 182040, HD 165929, and HD 100122, labelled 9, 10 and 11, respectively, in Fig. 2) exhibit variations with $\sigma_y > 10$ millimag, and probably represent unrecognized cases of variability caused by some external factor (like RS CVn, symbiotic, or R CrB variables...). The star HD 182040 for instance is a hydrogen-deficient carbon star, a family closely related to the R CrB variables (Feast & Glass 1973; Kilkenny et al. 1988). HD 100122 is a visual binary with a separation of $0''.38$ (Hartkopf et al. 1993; Horch et al. 1996) and a composite spectrum (G8/K0III + F; Houk & Cowley 1975);

(ii) Red giants become less and less stable as their $b - y$ index increases. Actually, a lower envelope to σ_y starts being noticeable for $b - y \gtrsim 0.8$ [as shown by the dashed line in Fig. 2a, referred to as the *minimum-variability boundary* in the following], such that no red giant seems to exist with σ_y below that limit (the three stars labelled 1, 2 and 3 in Fig. 2a are outliers because of their strong reddening, as shown in Sect. 4.1). It will be shown in Sect. 4.2 that *this increase of σ_y with increasing $b - y$ when $0.8 \leq b - y$ is not a spurious instrumental effect, but corresponds to the onset of real stellar variations with a time scale of 5 to 10 days*;

(iii) $b - y \geq 1.1$ (corresponding to spectral types M; Ardeberg & Lindgren 1985) marks the onset of large-amplitude variability ($\sigma_y \geq 0.010$ mag). Moreover, as will be shown in Sect. 5, the time scale of the underlying variations increases with their amplitude.

Photometric measurements are subject to various error sources (photon and scintillation noise, de-centering effects, short-term transparency variations...) that are not easy to evaluate, and that might possibly alter the $(\sigma_y, b - y)$ diagram presented in Fig. 2. In particular, the minimum σ_y of ~ 3 millimag observed for stars with $b - y \sim 0.6$ reflects the overall accuracy of our data. We stress, however, that all the other features observed in the $(\sigma_y, b - y)$ diagram as listed under items (i) to (iii) above reflect intrinsic stellar properties, as the detailed analysis presented in the next sections will show.

4. On the absence of stable red stars

In this section, the reality of the minimum-variability boundary represented by the dashed line in Fig. 2a, and corresponding to the minimum σ_y observed at a given $b - y$, will be assessed by showing first (Sect. 4.1) that the outlying position of the stars labelled 1, 2 and 3 in Fig. 2a is due to a strong reddening, and second (Sect. 4.2) that real stellar variations are responsible for the increase of σ_y along that boundary.

4.1. Reddening effects

Interstellar (and in some cases, even circumstellar) reddening increases the $b - y$ index of stars, thus shifting them towards the right in Fig. 2. The reddening suffered by a star can in principle

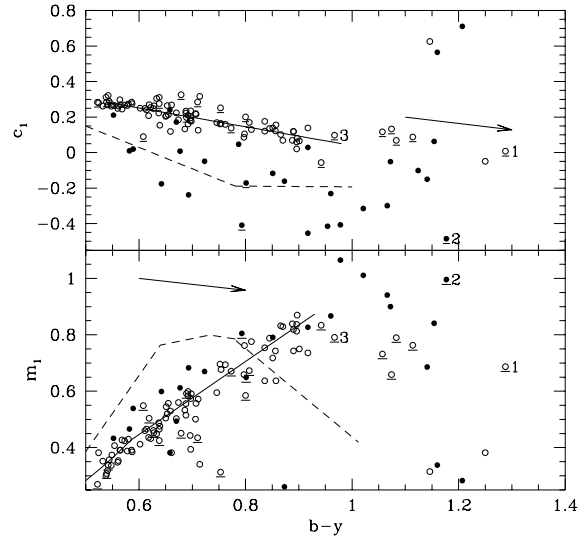


Fig. 3. The $(b - y, m_1)$ (lower panel) and $(b - y, c_1)$ (upper panel) diagrams for the sample of red giant stars extracted from the LTPV database as indicated in the text. Peculiar red giants (barium, S and carbon stars), whose photometric indices are altered by their chemical peculiarities, are represented by filled circles. Labels 1, 2 and 3 refer to the outlying stars in Fig. 2a (see text). Underlined symbols correspond to stars with $|b| < 10^\circ$ (b being the galactic latitude). The fiducial sequences for late-type main sequence stars and normal red-giant stars, as derived from Olsen (1984), are represented by the dashed and solid lines, respectively. The arrows indicate the reddening paths corresponding to $E_{b-y} = 0.2$ as given by Eq. (2)

be estimated from its position in the color-color diagrams $(b - y, m_1)$ and $(b - y, c_1)$ displayed in Fig. 3. In those diagrams, unreddened, non-chemically-peculiar red giant stars of solar metallicity fall on the fiducial sequences (represented by the solid lines in Fig. 3):

$$\begin{aligned} m_0 &= 1.269 (b - y)_0 - 0.30 \\ c_0 &= -0.528 (b - y)_0 + 0.57, \end{aligned} \quad (4)$$

derived from Olsen's (1984; his Figs. 8 and 9) sequences as described in Sect. 2. We note that the fiducial sequences defined by Eq.(4) are valid only for $(b - y)_0 \leq 0.95$. For larger $b - y$ values, the relative paucity of sample stars does not constrain the fiducial sequence well enough.

Interstellar reddening moves the stars away from the fiducial sequence along the reddening path according to Eq.(2), as represented by the arrows in Fig. 3.

The unreddened color indices can thus be derived from the intersection between the fiducial sequence and the reddening path passing through the observed indices, yielding the following expressions for the color excess E_{b-y} of non-peculiar red giants:

$$\begin{aligned} E_{b-y} &= 0.68 [-m_1 + 1.27 (b - y) - 0.30] \\ &= 5.78 [c_1 + 0.53 (b - y) - 0.57], \end{aligned} \quad (5)$$

provided that $(b - y)_0 \leq 0.95$. Since the Strömgren indices m_1 and c_1 depend upon metallicity (e.g. Gustafsson & Bell

Table 1. Reddening of stars with σ_y falling below the minimum-variability boundary in the $(\sigma_y, b - y)$ diagram (i.e. located to the right of the dashed line in Fig. 2a)

Name	LTPV	Sp.Type.	l	b	y	$b - y$	m_1	c_1	$E_{b-y}(m_1)$	$(b - y)_0$
Normal giants										
HR 7007	B7008	K4III	25	-2	5.811	0.967	0.791	0.098	0.09	0.88
HD 161406	B3014	K2III	2	0	8.627	1.288	0.687	0.008	0.44	0.85
PRG star										
HD 178717	P8004	K5Ba	44	0	7.150	1.177	0.996	-0.485	-	1.03 ± 0.05

1979), the above relations are in fact strictly valid only for solar-metallicity stars. For the two non-peculiar red giants HR 7007 and HD 161406 (labelled 3 and 1, respectively, in Fig. 2a), the color excess estimated from Eq. (5) is listed in Table 1, assuming a solar metallicity for these two stars. Since the reddening path runs almost parallel to the giant sequence in the $(b - y, c_1)$ diagram, the color excess estimated from that diagram is not very accurate, and has therefore not been listed in Table 1.

For HR 7007, the color excess $E_{b-y} = 0.09$ derived from the $(b - y, m_1)$ diagram yields $(b - y)_0 \simeq 0.88$. This brings the star right on the minimum-variability boundary.

For HD 161406, the color excess is found to be $E_{b-y} = 0.44$. This large value is not at all unexpected given the location of this star in the direction of the galactic center (see Table 1). According to Neckel & Klare (1980), the visual extinction A_V on that line of sight increases to about 3 mag (which corresponds to $E_{b-y} = 0.7$ adopting $A_V/E_{b-y} = 4.3$ from Crawford & Mandwewala 1976) over the first 600 pc. Adopting thus $E_{b-y} \sim 0.44$ leads to $(b - y)_0 \sim 0.85$, not unreasonable given its K2III spectral type (Ardeberg & Lindgren 1985) and bringing HD 161406 well above the minimum-variability boundary, as required if that boundary is to be real.

The third outlier, HD 178717, is a peculiar red giant. Because chemical peculiarities alter the colors (through e.g. stronger molecular bands), peculiar red giant stars are not expected to fall on the fiducial sequence. In particular, barium stars like HD 178717 have peculiar m_1 and c_1 indices due to the violet Bond-Neff depression (Bond & Neff 1969). The extinction maps provided by Neckel & Klare (1980) must thus be used instead of the color-color diagrams in order to estimate the color excess E_{b-y} . From the position of HD 178717 on these maps, it appears that the star lies at the edge of a region where the visual absorption A_V reaches 2.5 mag at 500 pc (field 264). Adopting $M_V = +1.0$ as a typical value for barium stars (Hakkila 1990), a distance of 100 to 200 pc is estimated for HD 178717, corresponding to a visual extinction A_V of the order of 0.5 to 1 mag. The corresponding reddening of 0.1 to 0.2 mag for HD 178717 brings its $(b - y)_0$ index close to the minimum-variability boundary.

A similar analysis for the stars lying on the minimum-variability boundary reveals that those stars *are not* heavily reddened, thus reinforcing the reality of that boundary. For instance, HD 60197 (labelled 4 in Fig. 2a), though close to the galactic

plane ($l = 244^\circ$ and $b = -5^\circ$), lies in a region (fields 85 and 90 of Neckel & Klare 1980) where the extinction remains low ($A_V < 0.2$ mag) over a distance of 1 kpc. The same holds true for HD 44896 (labelled 5 in Fig. 2a).

In conclusion, the reddening estimated for the three stars HD 161406, HR 7007 and HD 178717 makes it clear that their outlying position in Fig. 2a is an artifact due to their large color excess E_{b-y} . Their dereddened $(b - y)_0$ indices place them *above* the minimum-variability boundary, making the absence of stable red stars with $(b - y)_0 > 0.8$ quite striking (Fig. 2b).

4.2. Microvariability among red giants

Various instrumental effects causing a loss of accuracy for stars with extreme colors may be thought of to explain the absence of stable red stars in Fig. 2. In this section, it is instead argued that the minimum-variability boundary identified in Fig. 2a really reflects the growing stellar variability as a star gets redder.

In February 1994, two stars lying along the minimum-variability boundary, HD 60197 and HD 44896 (labelled 4 and 5, respectively, in Fig. 2a), have been observed once or twice per night during 15 consecutive nights. The corresponding lightcurves are presented in Fig. 4. Before February 1994, these stars were observed with a much sparser time sampling in the LTPV program (about 1 observation per week), and the resulting data gave the impression that the observed standard deviation of about 7 millimag resulted from random fluctuations of unknown origin. The lightcurves obtained with the nightly sampling of February 1994, however, clearly reveal low-amplitude variations on a time scale of 5 to 10 days.

The reality of the variations observed in February 1994 is ascertained by the much larger σ_y of $P - (A + B)/2$ as compared to that of $A - B$, by the clear trend of $P - (A + B)/2$ with time (see Fig. 4), and by the fact that two measurements performed a few hours apart during the same night give consistent results. Moreover, the fact that the variations of HD 60197 and HD 44896 are *uncorrelated* excludes a spurious instrumental origin for these variations and calls instead for their *stellar* origin. The similarity of the variations exhibited by HD 60197 and HD 44896, both in terms of amplitude and time scale, is nevertheless remarkable, and parallels the similarity of their $b - y$ indices.

The color indices $b - y$, m_1 and c_1 of HD 44896 and HD 60197 are also displayed in Fig. 4. They show no sign of

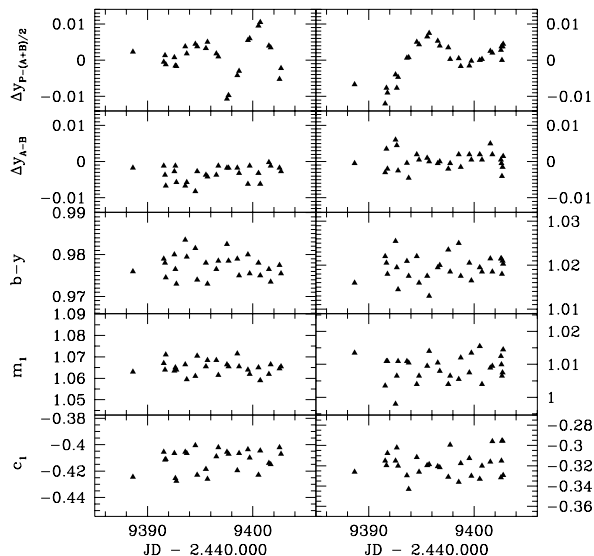


Fig. 4. Lightcurves of HD 44896 (left panel) and HD 60197 (right panel) in February 1994. *Upper panel:* differential magnitude $\Delta y_{P-(A+B)/2}$ in the y band. Negative values of $\Delta y_{P-(A+B)/2}$ correspond to the star P being fainter, whereas the zero point corresponds to the average differential magnitude over the whole monitoring. *Second panel from top:* same as the upper panel, but for the differential magnitude Δy_{A-B} . *Lower three panels:* lightcurves for the color indices $b - y$, m_1 and c_1 of the program star P

variability within the accuracy of the measurements over the 15 nights of the February 1994 run.

5. The period-amplitude relationship

In Sect. 3, a minimum variability level σ_y for red giant stars with a given $b - y$ index has been identified [the so-called ‘minimum-variability boundary’ observed in Fig. 2a]. In Sect. 4.2, it has been shown that stars lying along that boundary exhibit real variations with amplitudes of a few millimag on time scales of 5 to 10 d. In this section, we investigate the correlation between the time scale of the photometric variations and their amplitude. In addition to the two stars HD 44896 and HD 60197 having low-amplitude variations as discussed in Sect. 4.2, three stars with variations of larger amplitude (BD–08°1900, BD–21°5435 and BD–10°1334, labelled 6, 7 and 12, respectively, in Fig. 2b) are considered. They are the only large-amplitude variable stars in our sample with a lightcurve sampled well enough to perform a meaningful period analysis using the phase dispersion minimization (PDM) method (Stellingwerf 1978). For these three stars, the period search was performed by averaging the lightcurve over phase bins of length 0.2 overlapping by 0.1 phase units (i.e. $N_b = 5$, $N_c = 2$ following Stellingwerf’s notations).

BD–21°5435

The periodogram of BD–21°5435 is presented in Fig. 5, and reveals that the light variations are characterized by a time scale of the order of 37 d. As shown by the scatter present in the phase diagram, this period is, however, not quite stable from one cycle

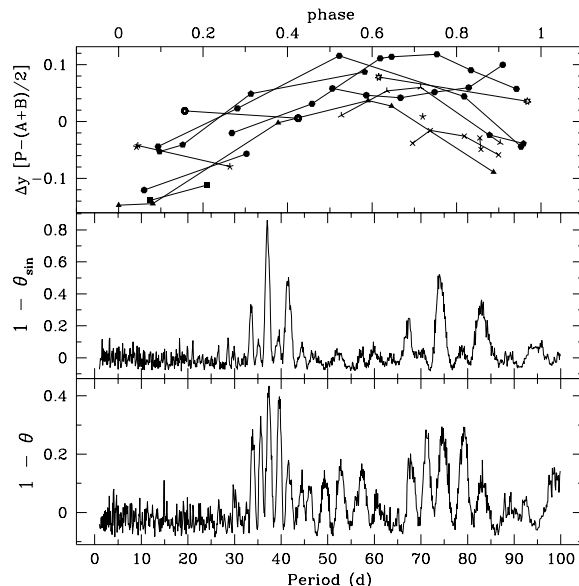


Fig. 5. *Lower panel:* Stellingwerf’s θ index for the differential magnitude $\Delta y_{P-(A+B)/2}$ of BD–21°5435 (defined as in Fig. 4), computed on phase bins of length 0.2 overlapping by 0.1 phase units. *Middle panel:* the θ index for a sine signal with a period 37.1 d sampled as the data. *Upper panel:* the differential y magnitude phased with the 37.1 d period. Data belonging to the same cycle have been connected

to the other. In a given cycle, the variations nevertheless follow a much more regular pattern than in the case of HD 44896 or HD 60197 (see Fig. 4).

BD–08°1900

The lightcurve of BD–08°1900 shown in Fig. 6 is similar to that of BD–21°5435, except for the somewhat longer time scale of the variations (of the order of 59 d, as compared to 37 d for BD–21°5435). This longer time scale goes along with a larger amplitude ($\sigma_y = 92$ millimag for BD–08°1900 as compared to 70 millimag for BD–21°5435).

BD–10°1334

The 117 d period present in the lightcurve of BD–10°1334 (Fig. 7) appears to be much more stable than the shorter time scales found for BD–08°1900 and BD–21°5435. Indeed, the various cycles spanning a total of 1120 d overlap almost perfectly in the phase diagram. This increased stability of the period of BD–10°1334 is again to be paralleled with the larger amplitude of its photometric variation (0.4 mag peak to peak) as compared to the other stars considered above.

The results obtained above are summarized in Table 2, and clearly show that, at least for the sample of red giants considered here, *the time scale of the light variations becomes longer as their amplitude increases, and the stability of this time scale improves concomitantly.*

6. Radial velocity variations

Radial-velocity data are of key importance for understanding the origin of the photometric variations of red giant stars dis-

Table 2. Comparison of the photometric amplitudes, photometric time scales, and radial-velocity amplitudes for five stars lying along the minimum-variability boundary. The effective temperature listed in column 4 has been derived from the spectral type – T_{eff} calibration of Ridgway et al. (1980), valid for S stars as well (Smith & Lambert 1990). P in column 7 is the time scale of the photometric variations. Columns 8 to 10 provide the radial velocity data, when available: σ_{v_r} , N and Δt are the radial-velocity standard deviation, number of measurements and time span, respectively. The last column lists the prediction for σ_y/σ_{v_r} based on a simple linear model for adiabatic acoustic oscillations from Kjeldsen & Bedding (1995; see Eq. 6). A colon identifies uncertain values

Name	LTPV	Sp. Typ.	T_{eff}	$b - y$	σ_y (millimag)	P (d)	σ_{v_r} (km s $^{-1}$)	N	Δt (d)	σ_y/σ_{v_r}	
										obs.	pred.
HD 44896	P8011	K5IIIBa	3980	0.979	6.8	$\sim 5 - 10$	< 0.2	19	3270	> 34	46
HD 60197	P8012	K3IIIBa	4260	1.022	7.7	$\sim 5 - 10$	< 0.2	13	3970	> 38	40
BD–21°5435	P8054	S3*4 ^a	3600	1.160	70.0	~ 37.1	–	–	–	–	56
BD–08°1900	P8040	S4/6 ^b	3500	1.348	92.0	~ 59.0	1.50	16	2630	61	59
BD–10°1334	P8050	S	3200: ^c	1.884	140.0	117.0	1.44	14	2317	97	71:

Notes:

a: S type from McConnell (1982), but listed as M3III in the Michigan spectral catalogue (Houk & Smith-Moore 1988);

b: Keenan & Boeshaar 1980;

c: assigned to type M6 given its very red color

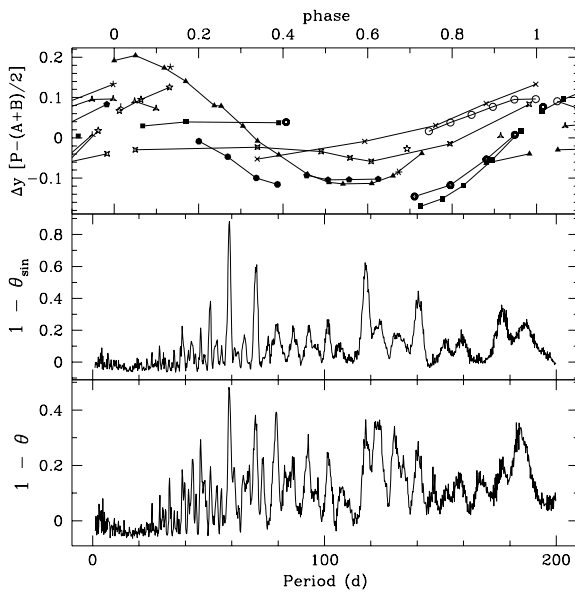


Fig. 6. Same as Fig. 5 for BD–8°1900. The differential y magnitude in the upper panel is phased with a 59.0 d period

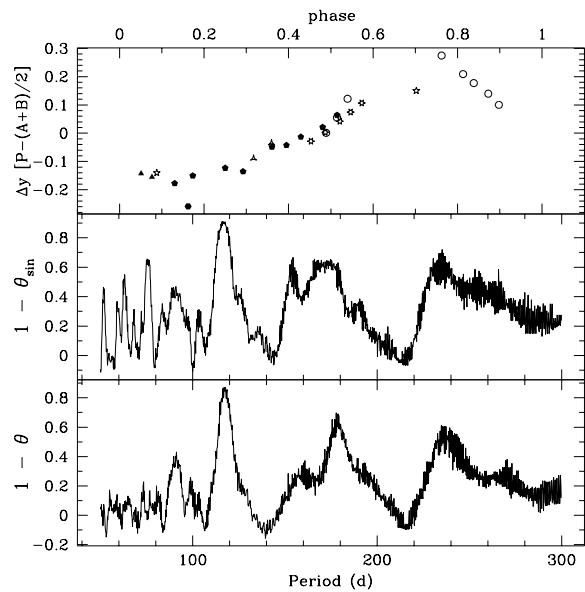


Fig. 7. Same as Fig. 5 for BD–10°1334. The differential y magnitude in the upper panel is phased with a 117 d period

cussed so far. Fortunately, such data are available for 4 among the stars listed in Table 2, as a result of the radial-velocity monitoring of barium and S stars performed with the CORAVEL spectro-velocimeter (Baranne et al. 1979) as described in Jorissen & Mayor (1988, 1992). The two barium stars HD 44896 and HD 60197 are in fact binary systems with orbital periods of 628.9 and 3200 d, respectively (Jorissen et al. 1997). For both stars, the standard deviation of the residuals around the orbital solution (0.2 km s^{-1}) is similar to the uncertainty on one measurement, so that no radial velocity jitter has in fact been detected at the level 200 m s^{-1} . However, radial-velocity variations of lower amplitude ($\leq 100 \text{ m s}^{-1}$) do exist in KIII stars (Hatzes

& Cochran 1994a and references therein). The radial-velocity variations of a well-studied star like Arcturus (α Boo, K2III) appear to be multiperiodic, with most periods below 10 d (Hatzes & Cochran 1994b). Since low-amplitude, irregular photometric variations on time scales of the same order are observed in HD 44896 and HD 60197, we speculate that these photometric variations are caused by the same physical mechanism (stellar pulsations, either radial or low-order non-radial?) as that responsible for the low-amplitude radial-velocity variations observed in Arcturus and other K giants.

The underlying radial velocity variations are in fact detected for the two S stars BD–10°1334 and BD–08°1900 analyzed in

Sect. 5. These stars do not show any sign of binary motion after more than 10 y of monitoring (Udry et al. 1997), but exhibit instead a significant radial velocity jitter of about 1.5 km s^{-1} (the third S star, BD-21°5435, is a long-period binary – $P > 2600 \text{ d}$ – whose orbit, and hence radial-velocity jitter, could not yet be determined). Unfortunately, the radial-velocity data are too sparse to be meaningfully correlated with the photometric data. Neither does a period analysis of the radial-velocity data using the PDM method pick up the photometric periods.

The significance of these results is briefly discussed in Sect. 7

7. Discussion

The results presented above provide important clues for a better understanding of the mechanisms causing the light variations in red giants. Somehow, the evolution of the light variability of these stars must reflect the evolution of their internal structure.

Several mechanisms may actually cause photometric variations in red giant stars, among which: (i) acoustic pressure-mode oscillations, excited either by the convective motions in the outer part of the star (‘solar-like oscillations’) or by the κ mechanism (as in Cepheid-like and Mira stars) (e.g. Kjeldsen & Bedding 1995), (ii) time-dependent surface inhomogeneities due to large convective cells (Schwarzschild 1975), or (iii) rotational modulation of stellar spots due to magnetic activity as in RS CVn variables.

It is beyond the scope of this paper to provide a definite conclusion as to which mechanism is responsible for the observed variations. Let us just remark that the detection of radial-velocity variations associated with the photometric variations probably favours an explanation in terms of radial or low-order non-radial oscillation modes, as already suggested by Hatzes & Cochran (1994b, 1996) for Arcturus and β Oph. In fact, from a simple linear theory of adiabatic acoustic oscillations, Kjeldsen & Bedding (1995) relate the standard deviation σ_λ (in millimag) of the light variations at wavelength λ (in nm) to the radial-velocity standard deviation σ_{v_r} (in km s^{-1}) caused by the oscillations by

$$\frac{\sigma_\lambda}{\sigma_{v_r}} = \frac{21.8}{(\lambda/550)(T_{\text{eff}}/5777)^2}. \quad (6)$$

Predictions based on this simple model are compared to the observations in Table 2, and show a fair agreement, indicating at least that this hypothesis appears to be a plausible one.

8. Conclusions

The main conclusions reached by the present study may be summarized as follows:

(i) The minimum variability level σ_y (where σ_y is the standard deviation of the Strömgren y magnitude) increases with increasing $b - y$ among red giants, thus defining a *minimum-variability boundary*. Red giants with spectral types late G to early K (i.e. $b - y \sim 0.6 - 0.8$; all $b - y$ values quoted here refer to intrinsic, dereddened indices) are all very stable ($\sigma_y < 6$ millimag),

in agreement with the results of previous studies (e.g. Grenon 1993; Eyer et al. 1994), whereas mid-K giants ($b - y \sim 0.8 - 1.0$) have $\sigma_y \sim 6$ millimag.

(ii) The value $b - y = 1.1$ (corresponding to early M spectral types) marks the onset of large-amplitude variability ($\sigma_y \geq 0.010 \text{ mag}$);

(iii) The time scale of the light variations increases with increasing $b - y$ and light amplitude, starting from about 10 d at the onset of stellar variability ($\sigma_y \sim 7$ millimag) and reaching 100 d at $\sigma_y \sim 0.1 \text{ mag}$;

(iv) The light variations are rather irregular at the onset of variability, but become more stable as the amplitude (or $b - y$) increases, reaching stable periods for P longer than about 100 d;

(v) There are indications that the light variations are associated with radial-velocity variations, thus suggesting an explanation of these variations in terms of radial or low-order non-radial stellar oscillations;

(vi) These conclusions apply to normal as well as to chemically-peculiar red giants. Despite the fact that chemical peculiarities make PRG stars appear redder than normal giants of the same T_{eff} , both families fall along the *same* minimum-variability boundary, thus suggesting that it is the atmospheric opacity as a whole (fixing $b - y$) and not T_{eff} alone that shapes the observed boundary.

These results call for further high-accuracy, simultaneous radial-velocity and photometric observations of K and M giants in order to clearly identify the physical mechanism underlying the microvariations exhibited by these stars.

Acknowledgements. This work was made possible thanks to the generous allotment of telescope time to the LTPV program by ESO. We thank M. Mayor and S. Udry for their help with the CORAVEL data. This research has made use of the SIMBAD database, operated at the Centre de Données Stellaires, Strasbourg, France. A.J. is Research Associate (F.N.R.S., Belgium). This work was written in part when A.J. was ‘Visiting Research Fellow’ at the Department of Astrophysical Sciences of Princeton University, whose hospitality is gratefully acknowledged. Financial support for this work has been provided by the *Fonds National de la Recherche Scientifique* (Belgium).

References

- Ardeberg A., Lindgren H., 1985. In: Hayes D.S., Pasinetti L.E., Davis Philip A.G. (eds.) *Calibration of Fundamental Stellar Quantities* (IAU Symp. 111). Kluwer, Dordrecht, p. 509
- Baranne A., Mayor M., Poncet J.L., 1979, *Vistas in Astronomy* 23, 279
- Bond E.H., Neff J.S., 1969, *ApJ* 158, 1235
- Crawford D.L., Mandwewala N., 1976, *PASP* 88, 917
- Edmonds P.E., Gilliland R.L., 1996, *ApJ* 464, L157
- Eyer L., Grenon M., Falin J.-L., Froeschlé M., Mignard F., 1994, *Solar Phys.* 152, 91
- Feast M.W., Glass I.S., 1973, *MNRAS* 161, 293
- Florentin Nielsen R., 1983, *Rep. Inst. Theor. Astrophys. Oslo* 59, 141
- Hakkila J., 1990, *AJ* 100, 2021
- Hartkopf W.I., Mason B.D., Barry D.J., McAlister H.A., Bagnuolo W.G., Prieto C.M., 1993, *AJ* 106, 352
- Hatzes A.P., Cochran W.D., 1994a, *ApJ* 432, 763

- Hatzes A.P., Cochran W.D., 1994b, ApJ 422, 366
Hatzes A.P., Cochran W.D., 1996, ApJ 468, 391
Horch E.P., Dinescu D.I., Girard T.M., van Altena W.F., 1996, AJ 111, 1681
Houk N., Cowley A.P., 1975. Michigan Catalogue of Two-Dimensional Spectral Types for the HD stars. Univ. Michigan, Ann Arbor, Vol. 1
Houk N., Smith-Moore M., 1988. Michigan Catalogue of Two-Dimensional Spectral Types for the HD stars. Univ. Michigan, Ann Arbor
Grenon M., 1993. In: Weiss W.W., Baglin A. (eds.) Proc. IAU Coll. 137, Inside the stars. Astron. Soc. Pacific Conf. Ser. 40, p. 693
Gustafsson B., Bell R.A., 1979, A&A 74, 313
Jorissen A., Mayor M., 1988, A&A 198, 187
Jorissen A., Mayor M., 1992, A&A 260, 115
Jorissen A., Van Eck S., Mayor M., Udry S., 1997, A&A, submitted
Keenan P.C., Boeshaar P.C., 1980, ApJS 43, 379
Kilkenny D., Marang F., Menzies J.W., 1988, MNRAS 233, 209
Kjeldsen H., Bedding T.R., 1995, A&A 293, 87
Manfroid J., Sterken C., Bruch A. et al., 1991, A&AS 87, 481
Manfroid J., Sterken C., Cunow B. et al., 1994, A&AS 109, 329
McConnell D.J., 1982, A&AS 48, 355
Neckel H., Klare G., 1980, A&AS 42, 251
Olsen E.H., 1984, A&AS 57, 443
Ridgway S.T., Joyce R.R., White M.M., Wing R.F., 1980, ApJ 235, 126
Schmitt J.L., 1971, ApJ 163, 75
Schwarzschild M., 1975, ApJ 195, 137
Smith V.V., Lambert D.L., 1990, ApJS 72, 387
Stellingwerf R.F., 1978, ApJ 224, 953
Sterken C., 1983, The Messenger 33, 10
Sterken C., 1994. In: C. Sterken, M. de Groot (eds.) The Impact of Long-Term Monitoring on Variable Star Research (NATO Advanced Research Workshop). Kluwer, Dordrecht, p.1
Sterken C., Manfroid J., 1992. Astronomical Photometry, a Guide. Kluwer, Dordrecht
Sterken C., Manfroid J., Anton K. et al., 1993, A&AS 102, 79
Sterken C., Manfroid J., Beele D. et al., 1995, A&AS 113, 31
Udry S., Mayor M., Jorissen A., Van Eck S., 1997, A&AS, submitted